# Gravity Waves in a Horizontal Shear Flow. Part II: Interaction between Gravity Waves and Potential Vorticity Perturbations

NIKOLAOS A. BAKAS AND BRIAN F. FARRELL

*Harvard University, Cambridge, Massachusetts*

(Manuscript received 4 May 2007, in final form 17 July 2008)

ABSTRACT

Interaction among potential vorticity perturbations and propagating internal gravity waves in a horizontally sheared zonal flow is investigated. In the strong stratification limit, an initial vorticity perturbation weakly excites two propagating gravity waves while the density component of the potential vorticity perturbation is significantly amplified, potentially leading to convective collapse. If stratification is sufficiently weak, a strong coupling between vorticity perturbations and gravity waves is found and spontaneous gravity wave generation occurs. This coupling can be traced to the nonnormal interaction between the potential vorticity and gravity wave manifolds in the weak stratification limit. Vorticity perturbations amplify in energy due to downgradient Reynolds stress when their phase lines tilt against the shear and the large growth attained is transferred to propagating gravity waves. When the flow geometry is such that the excited gravity waves are confined in the vicinity of the vorticity perturbation by their trapping levels, an overall convective collapse of this region can be anticipated. On the other hand, when the flow geometry permits wave propagation, significant gravity wave emission occurs.

## 1. Introduction

Mechanisms of internal gravity wave generation and breaking have been intensively studied because the internal wave field is ubiquitous in the ocean and also because of the role of internal wave energy generation and dissipation in the large-scale ocean circulation (Kuhlbrodt et al. 2007).

In Part I of this work (Bakas and Farrell 2009, hereafter Part I), we studied the evolution of small perturbations superposed on a stably stratified horizontal shear flow, focusing on the role of transient energy growth of perturbations with zero potential vorticity in producing breaking of gravity waves near the location where the wave intrinsic frequency approaches the Brunt–Väisälä frequency. In this second part, we study the interaction between potential vorticity perturbations and gravity waves and its role in spontaneous gravity wave generation and in producing conditions favorable for wave breaking.

Spontaneous generation of gravity waves has been studied previously in theoretical investigations of shallow-water equations (Ford 1994; Ford et al. 2000; Plougonven and Zeitlin 2002), of sheared disturbances on an $f$ plane (McWilliams and Yavneh 1998; Vanneste and Yavneh 2004; Kalashnik et al. 2006), and of Lorenz's five-component model (Vanneste 2004). Spontaneous emission of gravity waves has also been seen in observational studies (Uccellini and Koch 1987; Guest et al. 2000; Pavelin et al. 2001; Plougonven et al. 2003) and numerical simulations (O'Sullivan and Dunkerton 1995; Zhang 2004; Plougonven and Snyder 2007; Viudez and Dritschel 2006) of baroclinic life cycles. The term "spontaneous generation" refers to emission of gravity waves occurring abruptly during the evolution of an initially balanced flow as distinct from emission of gravity waves during geostrophic adjustment of an initially unbalanced flow. Ford et al. (2000) showed that in the small-Froude-number limit, emission of gravity waves is analogous to Lighthill radiation of acoustic waves (Lighthill 1952) and occurs due to frequency matching between the waves and the balanced motion. In the absence of such frequency matching, the emission is very weak, as found by Vanneste and Yavneh (2004), who showed that in the small-Rossby-number limit in

*Corresponding author address:* Nikolaos Bakas, National and Kapodistrian University of Athens, Office 32, Build IV, Panepistimiopolis, Zografos, Athens, Greece.
E-mail: nikos.bakas@gmail.com

DOI: 10.1175/2008JPO3837.1

which the balanced motions have low frequency compared to the internal wave frequency, the generated waves have an amplitude that is exponentially small in Rossby number.

In this work, we perform a generalized stability analysis (Farrell and Ioannou 1996) of a linear three-dimensional stably stratified model with a constant Brunt–Väisälä frequency and a meridional shear flow making use of closed-form asymptotic solutions. Our purpose is to clarify the role of potential vorticity perturbations and nonnormal interactions between vorticity and internal wave perturbations in the process of spontaneous wave generation and to assess the implications of this interaction for wave breaking.

This paper is organized as follows: in section 2, we describe the linear evolution of sheared disturbances in a stratified, barotropic horizontal shear flow and study the prototype growth mechanisms for potential vorticity perturbations. Section 3 describes the interaction between propagating gravity waves and potential vorticity perturbations. The role of nonnormality in the interaction between gravity waves and the vortical part of the flow is also investigated, and the optimal growing perturbations are identified to assess the effectiveness of interaction and energy transfer. In section 4, we study the emission of waves from a finite shear layer, and we finally end with a brief discussion in section 5 and our conclusions in section 6.

## 2. Growth mechanisms of horizontally sheared waves

The linearized, nondimensional equations governing the evolution of small perturbations to a stably stratified shear flow $\mathbf{U} = U(y)\hat{i}$ with constant buoyancy frequency in the vertical are given by (7) in Part I. In the next two sections, we follow the problem formulation in Part I in considering an unbounded, constant horizontal shear flow $U(y) = y$ in the absence of Rayleigh damping ($r = 0$). Assuming disturbances of the form $[\zeta, v, \rho] = [\hat{\zeta}(t), \hat{v}(t), \hat{\rho}(t)]\, e^{ikx+i(l-kt)y+imz}$, where $\zeta$, $v$, and $\rho$ are the meridional component of vorticity, meridional component of velocity, and density, respectively, allows reduction of the partial differential equations to the single second-order nonhomogeneous differential Eq. (10) of Part I for the evolution of density Fourier amplitude $\hat{\rho}(t)$. In Part I, solutions to the homogeneous restriction of this equation were studied, corresponding to perturbations without potential vorticity, and the growth mechanisms were identified in that case. In this study, we focus on the particular solution that describes the interaction between potential vorticity perturbations and gravity waves.

Before addressing the dynamics of three-dimensional perturbations, it is instructive to examine two separate two-dimensional limits: the first limit is to consider zonally independent perturbations, which addresses whether the mechanism of growth due to advection of zonal velocity studied in Part I is modified in the presence of potential vorticity perturbations; the second limit is to consider depth-independent motion. In this limit, potential vorticity and divergent waves are independent, and growth of potential vorticity perturbations can be studied in isolation.

### a. Growth of zonally uniform perturbations

Consider first the limit of zonally uniform perturbations ($k = 0$). In this case, it follows from (8) in Part I that the time-dependent Fourier components evolve in the absence of diffusion as

$$[\hat{\zeta}(t), \hat{v}(t), \hat{\rho}(t)] = \left[\hat{\zeta}(0) - \frac{im^2}{l}\hat{\rho}(0) + \hat{\zeta}_{\text{wave}}(t),\, \hat{v}_{\text{wave}}(t),\, \hat{\rho}_{\text{wave}}(t)\right], \quad (1)$$

where $\hat{\zeta}_{\text{wave}}(t), \hat{v}_{\text{wave}}(t), \hat{\rho}_{\text{wave}}(t)$ are given by (14)–(16) in Part I. These terms correspond to propagating gravity waves with zero potential vorticity that grow by advection of mean zonal velocity be perturbation meridional velocity to regions of higher/lower background velocity. The other two terms in (1) correspond to the nonpropagating initial potential vorticity perturbation that does not interact in this case with the propagating waves. Therefore, the energy evolution of a localized perturbation $[\zeta(y, z, t = 0), v(y, z, t = 0)] = [1, 1]\, A_v\, e^{-y^2/(\delta y)^2} \cos(mz)\cos(ly)$, which is shown in Fig. 1, has the same characteristics as the corresponding energy evolution of the localized perturbation having zero potential vorticity studied in Part I. The difference is that there is an additional contribution to the energy growth resulting, after the stage of wave interference, in an overall energy of $E = E_{\text{wave}} + E_q$, where

$$E_{\text{wave}} = \frac{1}{8}\left[\frac{m^2 + 2l^2 S}{l^2}|\hat{\rho}(0)|^2 + \frac{(l^2 + m^2)(m^2 + 2l^2 S)}{m^2 l^2 S}|\hat{v}(0)|^2\right]$$

is the contribution of propagating waves and

$$E_q = \frac{1}{4m^2}\left|\hat{\zeta}(0) - \frac{im^2}{l}\hat{\rho}(0)\right|^2$$

is the contribution of the nonpropagating potential vorticity perturbation to the total energy.

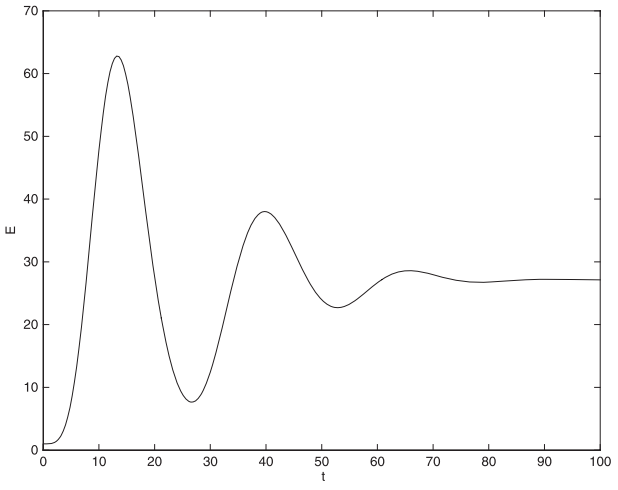


FIG. 1. Energy evolution of an initial wave packet perturbation $[\zeta(y,z,t=0),v(y,z,t=0)]=[1,1]A_v e^{-y^2/(\delta y)^2}\cos(mz)\cos(ly)$ determined by numerical quadrature of the Fourier integral (19) in Part I. Static stability is $S=1$, $(l, m)=(5,20)$, $\delta y=1.25$; $A_v$ is such that the initial wave packet has unit energy.

### b. The Orr mechanism

Consider now the case of solutions not varying in the vertical ($m=0$). It follows from system (8) in Part I that the time-dependent Fourier components evolve in the absence of diffusion as

$$[\hat{u}(t),\hat{v}(t)]=\left[-(l/k-t)\,\hat{v}(t),\frac{(k^2+l^2)\hat{v}(0)}{k^2+(l-kt)^2}\right],$$

$$[\hat{\zeta}(t),\hat{\rho}(t)]=[\hat{\zeta}(0),\hat{\rho}(0)]\cos(\sqrt{S}t)+\left[ik\sqrt{S}\hat{\rho}(0),\frac{i}{k\sqrt{S}}\hat{\zeta}(0)\right]\sin(\sqrt{S}t),$$

where $S$ is the nondimensional static stability.

There are two independent classes of solution: the horizontal velocity fields conserve the vertical component of vorticity, $\zeta_z=\partial_x v-\partial_y u$, leading to—due to kinematic deformation of $\zeta_z$ by the shear flow–transient growth of the cross-stream and streamwise velocity fields for waves with constant phase surfaces oriented against the mean shear. This is the mechanism of growth in two-dimensional shear discussed by Orr (1907), and we will refer to it as the Orr mechanism. Note that in this class of solutions, the motion is in the horizontal plane and growth is therefore unaffected by the buoyancy force. The second class of solutions is a buoyancy oscillation with the nondimensional Brunt–Väisälä frequency $S^{1/2}$. In the absence of initial perturbation variation in the vertical, there is no pressure gradient force in the vertical and therefore no coupling between horizontal and vertical velocities. The horizontal motions associated with potential vorticity and vertical motions are decoupled, and even though we have large energy growth of the vortical part of the flow, the transient amplification obtained cannot be sustained by excitation of buoyancy oscillations.

## 3. Evolution of three-dimensional perturbations

### a. Particular solution and gravity wave–vorticity wave interactions

The solution of the homogeneous Eq. (20) in Part I consists of propagating gravity waves with zero potential vorticity, which was studied in Part I. These waves asymptotically approach their trapping level where vertical velocity and density components oscillate with the nondimensional Brunt–Väisälä frequency resembling the buoyancy oscillations discussed in section 2b.

Here, we focus on the particular solution that is given by

$$\phi_{\text{part}}=\frac{ik\hat{q}(0)}{m}\phi_+\int_0^t\frac{\phi_-(s)a(s)}{W(s)}ds-\frac{ik\hat{q}(0)}{m}\phi_-\int_0^t\frac{\phi_+(s)a(s)}{W(s)}ds, \tag{2}$$

where $\phi_\pm$ are solutions to the homogeneous Eq. (20) in Part I,

$$W=\phi_+\frac{d\phi_-}{dt}-\phi_-\frac{d\phi_+}{dt}$$

is the corresponding Wronskian, $a(t)$ is given by (11) in Part I, and $\hat{q}(0)$ is the initial potential vorticity. We define $F=(m/k)/S^{1/2}$ as an inverse stratification parameter that depends on the vertical orientation of perturbations. There are two regimes depending on the parameter $F$ that are separated by the corresponding coupling strength between vorticity dynamics and gravity waves; we will study them separately.

#### 1) WEAK COUPLING ($F\ll 1$)

In contrast to the case with $m=0$, in this regime the nonzero pressure force in the vertical direction and coupling of horizontal and vertical velocity fields through the continuity equation produce a mixing of vorticity and divergent motion. The following question then arises: If we consider nondivergent initial conditions $[\hat{u}(0),\hat{v}(0),\hat{w}(0),\hat{\rho}(0)]=[-l/k,1,0,0]$, what portion of the initial energy will remain in the nonpropagating vorticity wave and what portion will radiate away as gravity waves? To address this question, we calculate the evolution of $\hat{\rho}(t)$ containing a vorticity and a gravity wave component: $\hat{\rho}(t)=\hat{\rho}_{\text{vort}}(t)+\hat{\rho}_{\text{wave}}(t)$.

Because in this regime perturbations have a weak vertical dependence [$(m/k) \ll S^{1/2}$], we expect to first order a behavior similar to the case $m = 0$ studied in section 2b, and we therefore seek a solution for the vorticity wave of the form: $\hat{\zeta}_z(t) = \zeta_0(t) + F^2\zeta_1(t) + F^4\zeta_2(t)\ldots$, where $\zeta_0(t) = \hat{\zeta}_z(0)$ corresponds to the $m = 0$ solution. Using conservation of potential vorticity in the absence of diffusion [(9) in Part I], it can be readily shown that this corresponds to seeking a solution of the form

$$\hat{\rho}_{\text{vort}}(t) = \frac{1}{S}\rho_1(t) + \frac{1}{S^2}\rho_2(t) + \cdots, \tag{3}$$

for the density perturbation of the vorticity wave. Using a similar expansion for $\hat{\rho}_{\text{wave}}(t)$, we show in appendix A that to leading order in $1/S$, the solution is

$$\hat{\rho}(t) = \hat{\rho}_{\text{vort}}(t) + \hat{\rho}_{\text{wave}}(t) = \frac{2k^2 m\hat{q}(0)}{iS[k^2 + (l - kt)^2]^2} + \frac{ik^2 m\hat{q}(0)\sqrt{\omega(t)}}{S(k^2 + l^2)^2\sqrt{\omega(0)}}\left[e^{i\sqrt{S}\int_0^t \sqrt{\omega(s)}ds} + e^{-i\sqrt{S}\int_0^t \sqrt{\omega(s)}ds}\right], \tag{4}$$

where $\omega$ is given by (12) in Part I and $\hat{q}(0) = i(k^2+l^2)/k$. The last two terms in (4) are the propagating gravity waves studied in Part I. In this weak coupling regime, these counterpropagating waves have a small amplitude [$O(F^2) \ll 1$] compared to the free-wave solution, as illustrated in Fig. 2, where the evolution of (2) is plotted.

The first term in the rhs of (4) is the first-order correction to the nonpropagating vorticity wave and corresponds to the large density amplification illustrated in Fig. 2, which might lead to a localized convective overturning of the vorticity perturbation. We note that expansion (3) is asymptotic rather than convergent as a result of exponentially small terms that it cannot capture. We show in appendix B that these terms represent propagating gravity waves excited abruptly at time $t = l/k$.

As in the case of sheared disturbances on the $f$ plane (Vanneste and Yavneh 2004), spontaneous generation of these gravity waves can be analyzed as an instance of a Stokes phenomenon (Olver 1974) in which the subdominant solution (waves) is switched on by the dominant solution (potential vorticity perturbation) when time crosses a Stokes line. To determine the leading-order approximation to the gravity wave amplitude, we now consider oscillation-free initial conditions; that is, we choose $\hat{\rho}(0) = \hat{\rho}_{\text{vort}}(0)$. We then follow the analysis in Vanneste and Yavneh (2004) in appendix B and use asymptotic matching in the complex $t$ plane (Hakim 1998) to show that the solution at large times is given by

$$\hat{\rho}(t) = \hat{\rho}_{\text{vort}}(t) + \frac{\hat{q}(0)\sqrt{\pi}e^{\sqrt{S}(i\phi_0 - \beta)}}{k\sqrt{2}S^{1/4}} \times \left[e^{i\sqrt{S}\int_0^t \sqrt{\omega(s)}ds} + e^{-i\sqrt{S}\int_0^t \sqrt{\omega(s)}ds}\right], \tag{5}$$

where $\phi_0$ and $\beta$ are given by (B4) and (B5), respectively. These spontaneously generated waves are exponentially small for large values of static stability being $O(e^{-\beta S^{1/2}})$, where $\beta$ is a function of $m/k$ bounded by one. In summary, the overall effect of potential vorticity perturbations in this regime is an amplification of density and vertical velocity of the nonpropagating vorticity wave and a weak excitation of propagating gravity waves. The amplitude of the gravity waves is $O(F^2)$ for nondivergent initial conditions and exponentially small in $1/S$ for oscillation-free initial conditions.

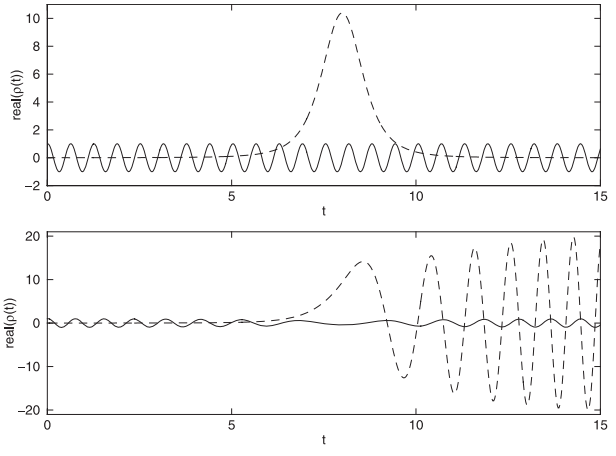


FIG. 2. Evolution of perturbation density for (top) $(k, l, m) = (1, 8, 0.01)$ and (bottom) $(k, l, m) = (1, 8, 5)$. The static stability is $S = 100$ and the initial conditions are $(\hat{\zeta}, \hat{v}, \hat{\rho}) = (-90i, 1.6, 1)$. The homogeneous solution given by (23) in Part I is shown by the solid line, and the particular solution given by (2) is shown by the dashed line.

### 2) STRONG COUPLING [$F\ O(1)$]

In this weak stratification regime, the amplitude of the spontaneously generated gravity waves is order one. The evolution of particular solution (2) with time for $m/k = 5$ is shown in Fig. 2 along with the free-wave solution. The forced waves' amplitudes remain at very low values until time $t = l/k = 8$. At that time, the large amplification of meridional velocity due to the Orr mechanism discussed in section 2b is transferred to

vertical velocity, exciting gravity waves. The amplitude of these forced waves increases rapidly and saturates at values much larger than the amplitude of the free-wave solution, as illustrated in Fig. 2. The amplitude of the forced waves is calculated in appendix C and is of order $\hat{q}(0)FS^{1/4}$ for $F$ $O(1)$, showing that a large initial potential vorticity perturbation leads to substantial excitation of waves. This linear coupling of vorticity perturbations and gravity waves in shear flow will now be further investigated.

### b. *Interaction between gravity wave and vorticity manifolds in a bounded shear flow*

In this section we trace the spontaneous generation of gravity waves by potential vorticity perturbations to the nonnormal interaction between the corresponding potential vorticity and divergent modes. If the modes are not orthogonal in the energy norm, mode interference allows energy extraction from the mean, leading to transient growth. We treat this problem by first calculating numerically the full viscous spectrum of the linearized operator governing the evolution of small perturbations to a shear flow in a channel $|y| \leq 2$. The linearized operator $\mathbf{A}$ is obtained by writing system (7) in Part I in the form

$$\frac{d\mathbf{x}}{dt} = \mathbf{A}\mathbf{x},$$

where $\mathbf{x} = [\tilde{\zeta}(y,t), \tilde{v}(y,t), \tilde{\rho}(y,t)]^{\mathrm{T}} e^{ikx+imz}$ is the state vector,

$$\mathbf{A} = \begin{pmatrix} -a_d + \frac{1}{\mathrm{Re}}\nabla^2 & -imU_y & ikS \\ 0 & \nabla^{-2}(-a_d\nabla^2 + \frac{1}{\mathrm{Re}}\nabla^4 + ikU_{yy} - r_y\partial_y) & imS\nabla^{-2}\partial_y \\ ik/(k^2+m^2) & (im/(k^2+m^2))\partial_y & -a_d + \frac{1}{\mathrm{Re}}\nabla^2 \end{pmatrix}, \tag{6}$$

$\nabla^2 = \partial_y^2 - (k^2 + m^2)$, and $a_d = (ikU + r)$. For simplicity, we perform the calculations for a constant shear flow $U = y$ in the absence of Rayleigh damping ($r = r_y = 0$). By discretizing the differential operators and incorporating the appropriate boundary conditions (zero meridional velocity and zero momentum and thermal fluxes at the boundaries), we interpret the above equation as a matrix equation in which the state becomes a column vector. The operator spectrum is then easily obtained by an eigenanalysis of matrix $\mathbf{A}$.

In the absence of viscosity and boundaries, the spectrum of $\mathbf{A}$ is continuous and consists of a real number infinity of singular neutral modes, which are replaced by a countable discrete spectrum of analytic modes in the viscous case. The spectrum of the analytic modes of $\mathbf{A}$ is shown for $(k, m, S) = (1, 0.001, 1)$ in Fig. 3. Because diffusion is proportional to the second derivative in $y$, the real parts of the frequencies are ordered according to the meridional wavelength of the modes, with longer wavelengths at the top of the spectrum. We observe three distinct Y-shaped branches shown by dots, crosses, and open circles. The tail of the middle branch consists of modes with zero frequency, corresponding to the nonpropagating potential vorticity modes. The tails of the left and right branches consist of modes having frequencies close to the nondimensional Brunt–Väisälä frequency and correspond to the two branches of gravity waves. The structure of one of the vorticity manifold modes is shown in Fig. 4. This structure results from balance between the tendency of shear to increase the meridional wavenumber and diffusion to decrease it. The structure of the gravity wave modes is similar but displaced toward the trapping level.

To study the interaction among the modes in each manifold and between manifolds, we separate the three branches with the modes increasing in frequency. We then calculate the measure of energy orthogonality among the modes $E_{ij} = \mathbf{x}_i^{\dagger}\mathbf{M}\mathbf{x}_j$, where $\mathbf{x}_i$ is the state vector of the $i$th mode, $\dagger$ denotes the complex conjugate, and

$$\mathbf{M} = \frac{\Delta y}{4(k^2+m^2)} \begin{bmatrix} 1 & 0 & 0 \\ 0 & k^2+m^2-\partial_y^2 & 0 \\ 0 & 0 & S(k^2+m^2) \end{bmatrix} \tag{7}$$

is the energy metric, with $\Delta y$ the grid interval. A histogram of $E_{ij}$ is shown in Fig. 5 for the gravity wave (Fig. 5a) and vorticity (Fig. 5b) manifolds. If the modes were orthogonal, $E_{ij}$ would be the identity. Because $E_{ij}$ is concentrated near the diagonal, we conclude that only neighboring modes interact strongly within each manifold, with the upper part of the spectrum containing larger wavelengths dominating the energetic interaction. The result of nonorthogonality in each of the manifolds and of nonnormal interference among modes is the observed transient energy growth of both vorticity (studied in section 2b) and gravity waves (studied in Part I). The coupling between the two gravity wave branches is illustrated in Fig. 5c and between gravity

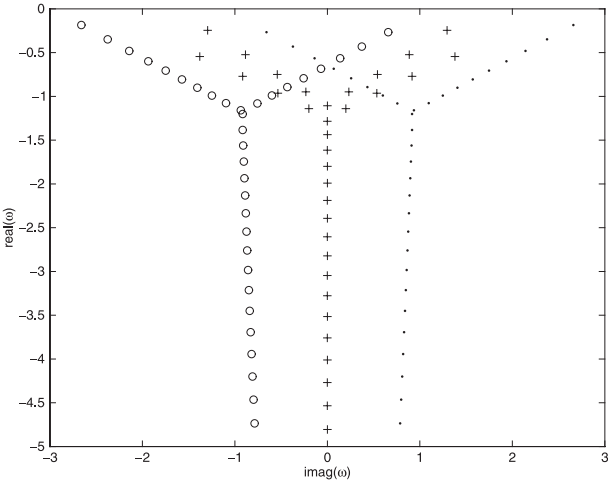


FIG. 3. The spectrum of the analytic modes of a constant shear flow in a channel $|y| \leq 2$. The zonal and vertical wavenumbers are $(k, m) = (1, 0.001)$, the static stability is $S = 1$, and the Reynolds number is $\mathrm{Re} = 150$.

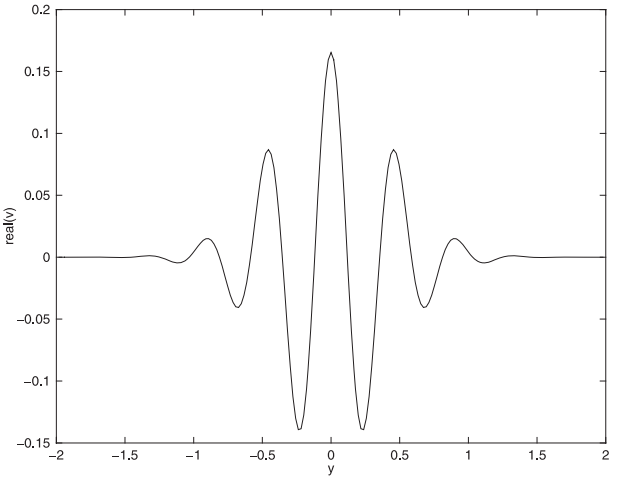


FIG. 4. Real part of the meridional velocity of the mode with frequency $\omega = 0 + 1.28i$.

wave and vorticity manifolds in Fig. 5d. We can see that gravity wave and vorticity manifolds are almost orthogonal in this case, as we are in the weak coupling regime ($F \ll 1$), with the two gravity wave manifolds being almost orthogonal as well. Inspection of the modes reveals that orthogonality between vorticity and gravity wave manifolds arises in this case because almost all of the energy in vorticity modes is contained in meridional velocity, whereas almost all of the energy in gravity waves is in density and vertical velocity. The result of this near orthogonality is that vorticity perturbations and gravity waves evolve independently with a very weak excitation of gravity waves by potential vorticity perturbations, as discussed in the previous section.

The corresponding histograms of energy orthogonality $E_{ij}$ for $(k, m, S) = (1, 1, 1)$ are shown in Fig. 6 with similar features in orthogonality within each manifold. But because we are in the strong coupling regime [$F\,O(1)$], there is strong projection of vorticity modes on gravity wave modes consistent with a substantial energy growth when these modes are optimally configured as an initial condition in the shear flow.

### c. Optimal perturbations

In previous sections we found that vorticity perturbations and gravity waves interact strongly for $F\,O(1)$. Vorticity perturbations that grow transiently due to the Orr mechanism transfer their amplified energy to propagating gravity waves, while gravity waves can also benefit from the synergy between downgradient Reynolds stresses and growth due to zonal advection, as studied in Part I. To determine the effectiveness of energy transfer to gravity waves and to obtain a constructive upper bound for the overall transient energy growth, we calculate in this section the initial conditions yielding the largest energy amplification over a specified time interval $T_{\mathrm{opt}}$.

A complete analysis proceeds from first writing system (8) in Part I in the compact form

$$\frac{d\chi_q}{dt} = \mathbf{B}_q(t)\chi_q, \tag{8}$$

where $\chi_q$ is the column vector $\chi_q = [\hat{\zeta}, \hat{v}, \hat{\rho}]^{\mathrm{T}}$ and $\mathbf{B}_q(t)$ is

$$\mathbf{B}_q(t) = \begin{pmatrix} -\frac{K(t)^2}{\mathrm{Re}} & -im & ikS \\ 0 & \frac{2k(l-kt)}{K(t)^2} - \frac{K(t)^2}{\mathrm{Re}} & \frac{m(l-kt)S}{K(t)^2} \\ \frac{ik}{k^2+m^2} & -\frac{m(l-kt)}{k^2+m^2} & -\frac{K(t)^2}{\mathrm{Re}} \end{pmatrix}.$$

We then express (8) in terms of the new variable $\mathbf{y} = \mathbf{M}_E^{1/2}\chi_q$, where $\mathbf{M}_E$ is the energy metric

$$\mathbf{M}_E = \frac{1}{4(k^2+m^2)} \begin{bmatrix} 1 & 0 & 0 \\ 0 & K(t)^2 & 0 \\ 0 & 0 & S(k^2+m^2) \end{bmatrix},$$

for which perturbation energy is given by the inner product: $E = \mathbf{y}^{\dagger}\mathbf{y}$. The governing equations are then transformed to

$$\frac{d\mathbf{y}}{dt} = \mathbf{D}\mathbf{y},$$

where the time-dependent matrix $\mathbf{D}(t)$ is

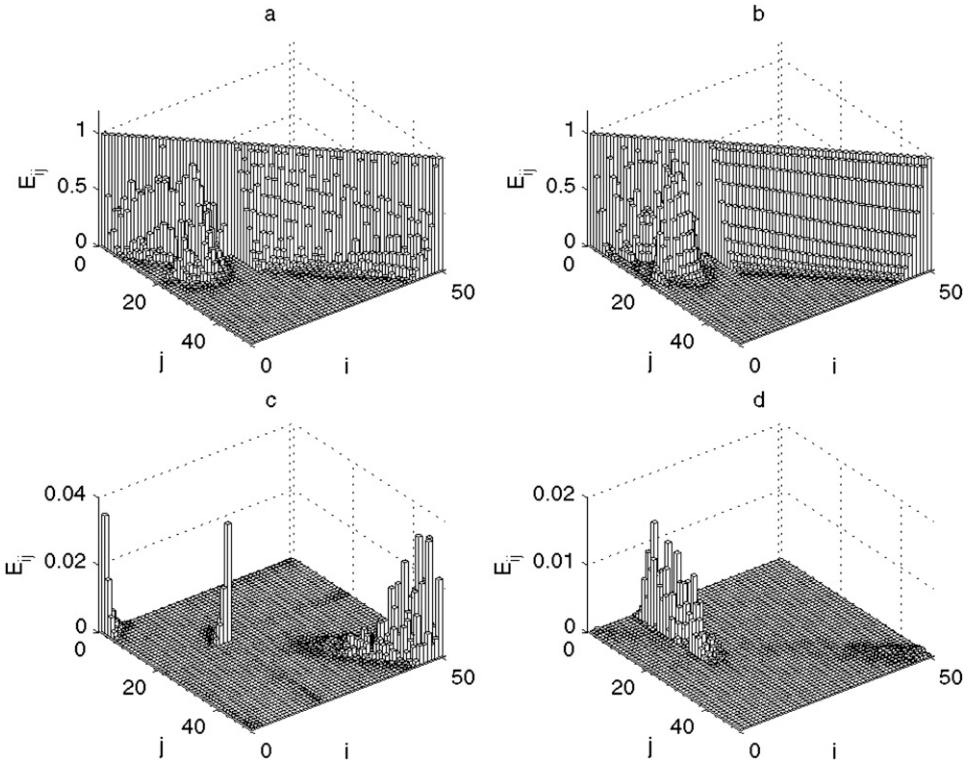


FIG. 5. Histogram of the measure of energy orthogonality among the modes $E_{ij} = \mathbf{x}_i \dagger \mathbf{M}_j$, where $\mathbf{x}_i$ is the state vector of the $i$th mode and $\mathbf{M}$ is the energy metric given by (7). (a), (b) The $E_{ij}$, where both $\mathbf{x}_i$ and $\mathbf{x}_j$ belong to the left (gravity wave) and middle (vorticity) Y-shaped branches shown in Fig. 3, respectively. Here, $E_{ij}$ is symmetric and only values for $j > i$ are shown. (a) The extent of energy nonorthogonality among the gravity wave modes of each branch, and (b) the nonorthogonality of the vorticity modes. (c), (d) The $E_{ij}$, where $\mathbf{x}_i$ belongs to the left branch (gravity wave manifold) and $\mathbf{x}_j$ belongs to the right (gravity wave manifold) and middle (vorticity manifold) Y-shaped branches shown in Fig. 3, respectively. (c) The energy nonorthogonality between the gravity wave mode branches and (d) between the gravity modes and the vorticity modes. The zonal and vertical wavenumbers are $(k, m) = (1, 0.001)$, static stability is $S = 1$, and the Reynolds number is $\mathrm{Re} = 150$.

$$\mathbf{D}(t) = \left( \frac{d\mathbf{M}_E^{1/2}}{dt} + \mathbf{M}_E^{1/2} \mathbf{B}_q \right) \mathbf{M}_E^{-1/2}.$$

As discussed in Part I, for a given set of wavenumbers, $(k, l, m)$, singular-value decomposition of the finite-time propagator $\mathbf{\Phi}(t)$ mapping the initial perturbation to its state at time $t$ identifies the optimal initial conditions and the corresponding growth $E_{\mathrm{opt}}^{klm}(T_{\mathrm{opt}})$. The perturbation growing the most is then obtained numerically by a descent algorithm determining the wavenumbers $(k, l, m)$ maximizing $E_{\mathrm{opt}}^{klm}(T_{\mathrm{opt}})$ and the corresponding growth is $E_{\max} = \max_{klm}[E_{\mathrm{opt}}^{klm}(T_{\mathrm{opt}})]$.

For an unbounded shear flow, there is no intrinsic space scale, and in the inviscid limit the solutions along with the energy amplification depend only on the ratios $l/k$ and $m/k$—wavenumber maximization proceeds by maximization over these two ratios. The optimal energy growth $E_{\max}$ achieved at $T_{\mathrm{opt}}$ as a function of the optimization time $T_{\mathrm{opt}}$, for static stability $S = 1$ and $S = 100$ is shown in Fig. 7. The growth achieved is much larger compared to the corresponding growth in the absence of potential vorticity perturbations (cf. Part I), suggesting that it is the result of strong vorticity perturbations–gravity wave interactions.

The optimal perturbations are configured in such a way as to exploit the Orr mechanism for transient amplification of vorticity perturbations while enabling the effective transfer of energy to gravity waves. Therefore, their initial horizontal tilt $l/k \leq T_{\mathrm{opt}}$ is such that the plane wave assumes a cross-stream orientation $(\tilde{l}/k = l/k - t = 0)$ at a time $t \leq T_{\mathrm{opt}}$ to benefit from the intensification of meridional velocity. In addition, their vertical orientation is of order $(m/k)$ $O$ $(S^{1/2})$, so that there is a strong coupling between vorticity perturbations and gravity waves, and their energy is concentrated predominantly in zonal velocity to maximize the gain from vorticity dynamics. Because the forced waves'

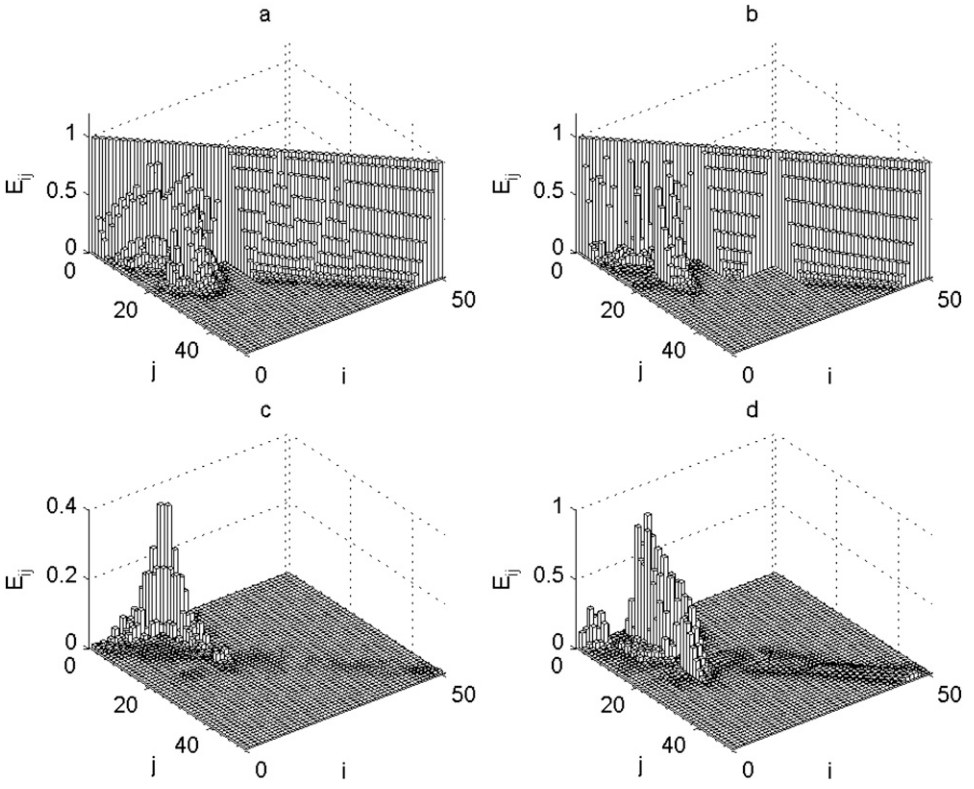


FIG. 6. Same as in Fig. 5, but for zonal and vertical wavenumbers $(k, m) = (1, 1)$. These histograms reveal enhanced nonorthogonality among the gravity wave modes and the vorticity modes at this higher vertical wavenumber.

amplitude is of order $\tilde{q}(0)FS^{1/4}$ and $F\,O(1)$, the optimal growth is enhanced by larger static stability, as seen in Fig. 7.

Viscosity breaks the scale invariance, as we implicitly select an intrinsic scale by choosing the Reynolds number. As in Part I, in the absence of an intrinsic scale for unbounded flow, the Reynolds number in this section is prescribed for a given coefficient of viscosity on perturbations having unit zonal wavenumber ($k = 1$). This arbitrary choice of Reynolds number disappears when a spatial scale is provided, as in the next section. The optimal growth as a function of optimizing time is shown in Fig. 8 for static stability $S = 1$ and $S = 100$ and for $\mathrm{Re} = 10^3$ and $\mathrm{Re} = 10^5$. Viscosity limits the energy amplification but does not essentially alter the characteristics of the inviscid optimal perturbations for small optimization times. The optimal growth has a maximum that increases with Reynolds number, as illustrated in Fig. 8. The optimization time $T_{\mathrm{opt}}$ at which the maximum is attained is $O(\mathrm{Re}^{1/3})$, consistent with the $e$-folding time of $O(\mathrm{Re}^{1/3})$ of vorticity dynamics (Bakas et al. 2001). Moreover, unlike in the inviscid case, for optimization times larger than $\mathrm{Re}^{1/3}$, $l/k < T_{\mathrm{opt}}$ because there is rapid viscous dissipation associated with the high meridional wavenumber perturbations lying nearly in the zonal direction.

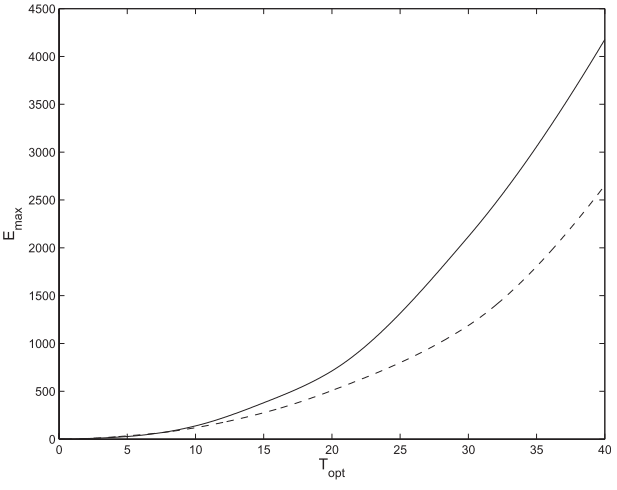


FIG. 7. The optimal energy growth $E_{\mathrm{max}}$ achieved at $T_{\mathrm{opt}}$ as a function of the optimization time $T_{\mathrm{opt}}$ for static stability $S = 100$ (solid line) and $S = 1$ (dashed line). The flow is inviscid.

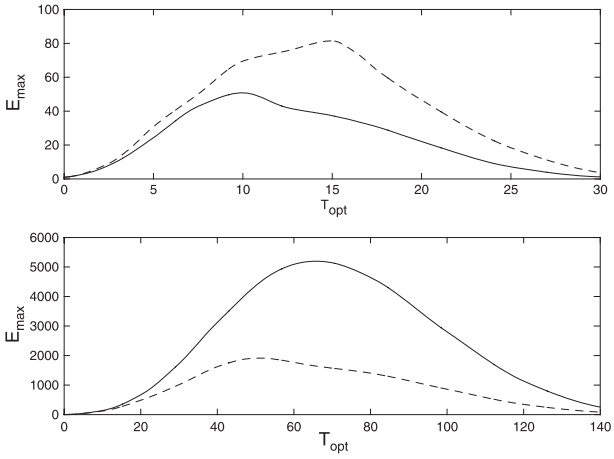


FIG. 8. (top) The optimal energy growth $E_{\max}$ as a function of the optimization time $T_{\text{opt}}$ for static stability $S = 100$ (solid line) and $S = 1$ (dashed line). The Reynolds number is $\text{Re} = 10^3$. (bottom) The optimal energy growth $E_{\max}$ as a function of the optimization time $T_{\text{opt}}$ for static stability $S = 100$ (solid line) and $S = 1$ (dashed line). The Reynolds number is $\text{Re} = 10^5$.

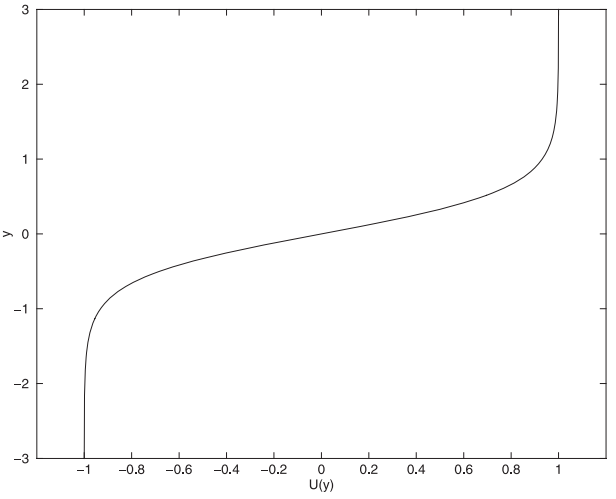


FIG. 9. Meridional velocity profile (9), where $\delta y = 0.6$.

## 4. Emission of gravity waves from a shear layer

As discussed in the previous section, excitation of gravity waves by potential vorticity perturbations is robust for $F\,O(1)$, leading to a large energy transfer to propagating waves. While in a constant shear flow these waves are bounded by their trapping levels, in a flow with shear varying with latitude, the possibility arises that the energy in gravity waves may propagate away and lead to enhanced gravity wave activity in remote regions. To investigate this possibility, we use the mean velocity profile

$$U(y) = \tanh\left(\frac{y}{\delta}\right), \tag{9}$$

shown in Fig. 9. It consists of a region of shear flow bounded by two regions of uniform velocity. The length and velocities used to nondimensionalize the equations are the shear $\alpha = 1/\delta$ and the difference in velocities of the upper and lower regions $V_0 = 2$. The Reynolds number based on the selected scale is $\text{Re} = 10^3$. Radiation conditions are imposed by inserting sponge layers at the top and bottom of the domain through the introduction of meridionaly varying Rayleigh damping:

$$r(y) = a_r\{1 + \tanh[(y - y_{\text{upper}})/\delta_r]\} + a_r\{1 - \tanh[(y - y_{lower})/\delta_r]\},$$

in which $a_r$ is the damping amplitude of the sponge layer, $y_{\text{upper}}$ and $y_{\text{lower}}$ are the latitudes of the sponge, and $\delta_r$ determines the transition width into the sponge layer. We have selected sponge-layer parameter values that result in no appreciable spurious back reflection from variation of $r(y)$.

To address the question of what portion of energy deposited into propagating waves remains trapped in the shear layer and what portion radiates to infinity, we perform the following optimization: we calculate the initial perturbation of unit energy, which is confined inside the shear layer and which leads to the largest energy within a region above/below the shear layer at a specified time $T_{\text{opt}}$. To obtain the optimal perturbations, we introduce two projector matrices $\mathbf{M}_s$ and $\mathbf{M}_t$ with nonzero diagonal elements corresponding to $|y| \le 1.5$ and $2 \le |y| \le 4$, respectively. For a given set of wavenumbers, $(k, m)$, the singular value decomposition of $\mathbf{M}_t^{1/2} e^{\mathbf{A}T_{\text{opt}}} \mathbf{M}_s^{-1/2} = \mathbf{U}\mathbf{V}^{\dagger}$, where $\mathbf{A}$ and $\mathbf{M}$ are given by (6) and (7), respectively, identifies the optimal perturbation $\mathbf{x}_{\text{opt}}$ as the first column of $\mathbf{M}_s^{-1/2}\mathbf{V}$, with energy growth, $E_{km}$, given by the square of the corresponding singular value. The perturbation growing the most is then obtained numerically by a descent algorithm determining the wavenumbers $(k, m)$ maximizing $E_{km}$. Our search is restricted in the range of $(k, m)$ for which the shear layer is Kelvin–Helmholtz stable.

Performing the optimization for various values of static stability, we find that the vertical orientation is again of order $(m/k)\ O(S^{1/2})$, yielding $F\,O(1)$ and utilizing the transfer of growth from vorticity perturbations to propagating gravity waves. The energy evolution inside and outside of the shear layer for the optimal perturbation $\mathbf{x}_{\text{opt}}$ is given by

$$E_{\text{in}} = \mathbf{x}_{\text{opt}}^{\dagger} e^{\mathbf{A}^{\dagger} t} \mathbf{M}_s \mathbf{M} e^{\mathbf{A}t} \mathbf{x}_{\text{opt}},$$

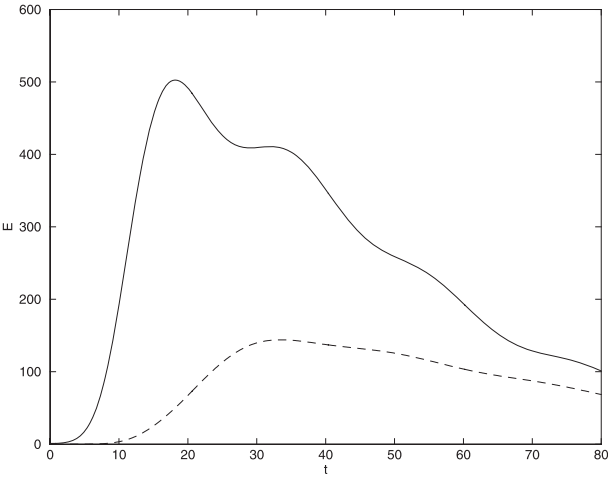


FIG. 10. Energy evolution of the optimal initial perturbation having $(k, m) = (1, 1)$. The solid line shows the energy within the shear layer ($|y| \leq 1.5$) and the dashed line shows the energy outside of the shear ($2 \leq |y| \leq 4$). The static stability is $S = 1$, the Reynolds number is $\mathrm{Re} = 10^3$, and the optimization time is $T_{\mathrm{opt}} = 30$.

$$E_{\mathrm{out}} = \mathbf{x}_{\mathrm{opt}}^{\dagger} e^{\mathbf{A}^{\dagger} t} \mathbf{M}_t \mathbf{M} e^{\mathbf{A} t} \mathbf{x}_{\mathrm{opt}},$$

respectively, and is shown in Fig. 10 for $S = 1$. A large amplification occurs within the shear layer followed by wave excitation, and around 30% of the energy is radiated away, leading to substantial emission of wave activity. Because half of the observed growth within the shear is attributed to potential energy increase, we anticipate for sufficiently large initial perturbations a localized convective collapse at some stage of the evolution. The result expected would therefore be a turbulent collapse in the shear region, accompanied by a substantial emission of waves. Further investigation is needed, however, in the nonlinear regime to verify this hypothesis and examine the amount of emitted energy before the shear collapse.

## 5. Discussion

We now relate the results obtained in this work to previous theoretical studies. Gravity wave excitation by sheared disturbances has been intensively investigated in the past for perturbations in a meridional shear flow on an *f* plane using numerical integrations (McWilliams and Yavneh 1998; Kalashnik et al. 2006) and analytic solutions (Vanneste and Yavneh 2004).

Vanneste and Yavneh (2004) addressed spontaneous inertia–gravity wave generation by initially balanced motion and identified three regimes: the small-Rossby-number regime, in which gravity waves and balanced motion have the same scale but different frequencies; the small-Froude-number regime, in which there is no frequency separation between waves and balanced motion but gravity waves are generated with a much larger spatial scale analogous to Lighthill radiation; and the regime of both Rossby and Froude numbers of order one, in which the waves and the balanced motion have frequencies and spatial scales of the same order. Vanneste and Yavneh (2004) addressed wave generation in the small-Rossby-number regime and found that wave amplitudes were exponentially small in Rossby number because of frequency separation between inertia–gravity waves and balanced motion. In our study, frequency separation between gravity waves and potential vorticity perturbations for $(m/k) \ll S^{1/2}$ resulted in an exponentially small amplitude as well, supporting Vanneste and Yavneh's (2004) conclusion that an exponentially small amplitude for the generated gravity waves is expected in cases of frequency separation.

Vanneste and Yavneh (2004) also noted that in the absence of such separation (as in the low-Froude-number regime), the wave amplitudes follow a power law in Froude number (Ford et al. 2000). They finally briefly discussed the third asymptotic regime of Rossby and Froude numbers of order one. Based on scaling arguments and numerical integrations, they deduced that the wave amplitude for $m/k$, $S \gg 1$ and $(m/k)$ $O(S^{1/2})$, scales like $S^{1/4}$. This result was verified in our study in the absence of rotation, using analytic solutions. It shows that a power-law dependence on the asymptotic parameter appears in the case of incomplete frequency separation between vorticity perturbations and divergent motions, regardless of whether there is spatial separation and a Lighthill-like radiation mechanism.

McWilliams and Yavneh (1998) also studied the evolution of sheared disturbances on an *f* plane, focusing on a completely different aspect: they related gravity wave excitation to the loss of semiellipticity of the resulting differential equations occurring when the condition

$$f + (\partial_x v - \partial_y u) - \sqrt{(\partial_x u - \partial_y v)^2 + (\partial_y u - \partial_x v)^2} > 0 \tag{10}$$

is violated for some time interval. This marginal condition involving the absolute vorticity and the magnitude of strain rate associated with horizontal velocity gradients occurs in between the regimes of inertial and symmetric instability and does not necessarily imply exponential growth of small perturbations. Numerical tests showed that (10) is violated for $F$ $O(1)$ in our case and also indicated that this condition is related to the coupling of vorticity and divergent manifolds. Furthermore, following a heuristic conjecture along with numerical tests, McWilliams and Yavneh (1998) were able

to obtain the vorticity perturbation for which the wave amplitude was maximum. The optimal condition for wave excitation was found to be $(m/k)S^{-1/2} = 3\pi/8$, a result verified in our study with the use of a rigorous optimization calculation.

In summary, qualitative and quantitative agreement of our results with those of previous studies of gravity wave generation by initially balanced motion on an $f$ plane shows that the basic features of the excitation mechanism of gravity waves by the sheared vorticity waves investigated in this study remain unaltered by rotation. However, in addition to highlighting the role of frequency matching between the vorticity manifold and the gravity wave manifold in the coupling between them, this work directly linked spontaneous generation of gravity waves by potential vorticity perturbations to the nonnormal interaction between the corresponding potential vorticity and divergent manifolds. As a result, the energy orthogonality among the modes can be used as a diagnostic for wave excitation in realistic situations, unlike an asymptotic theory providing the gravity wave amplitude, whose derivation is likely to be challenging in the general case.

## 6. Conclusions

Interaction between nonpropagating potential vorticity perturbations and internal gravity waves within a meridionally varying shear flow was investigated. For zonally and vertically independent solutions, potential vorticity perturbations and gravity waves grow transiently but without energy transfer between them, as they evolve independently. For strong stratification [$F = (m/k)/S^{1/2} \ll 1$], a weak coupling was found, leading to gravity wave excitation by vorticity perturbations. In the case of oscillation-free initial conditions, while the density field of the potential vorticity perturbation was significantly amplified, potentially leading to local convective overturning, two counterpropagating gravity waves with an exponentially small amplitude $O[\exp(-\beta S^{1/2})]$ were spontaneously generated through a Stokes phenomenon.

For weak stratification [$F\,O(1)$], a strong coupling was found as was a robust gravity wave excitation by vorticity perturbations. Unlike previous studies linking wave excitation either to the absence of frequency separation between the slow vorticity manifold and gravity waves (Vanneste and Yavneh 2004) or to the loss of semiellipticity of equations occurring when the modulus of horizontal strain rate exceeds the absolute vorticity (McWilliams and Yavneh 1998), this work highlighted the link of strong coupling to nonnormal interaction between potential vorticity and gravity wave manifolds and focused on the mechanisms of growth and energy transfer using analytic solutions and variational methods. Vorticity perturbations were found to amplify due to the Orr mechanism when their phase lines are tilted against the shear ($l/k > 0$) and the energy acquired is then transferred to gravity waves excited at $t \sim l/k$ through a Stokes phenomenon. These spontaneously generated waves finally emerge with an amplitude of order $\hat{q}(0)FS^{1/4}$. Calculation of optimally growing perturbations verified that this wave-excitation mechanism can lead to robust energy growth that is effectively transferred to propagating gravity waves. The most effective energy transfer was found for perturbations having $(m/k)$ $O(S^{1/2})$, in agreement with the results of McWilliams and Yavneh (1998).

For an unbounded shear, all of the wave activity is confined in a region determined by the waves' trapping levels, and convective collapse of this region is expected according to our findings in Part I. For a finite shear layer, a significant amount of wave activity was also found to be emitted from the shear layer. Although extension of these results to the nonlinear regime is needed to investigate breaking and subsequent turbulent mixing, the mechanism of growth and wave excitation examined in this paper is expected to play a significant role in mixing.

In addition, agreement of our results with the findings of previous studies of gravity wave generation by balanced motion (McWilliams and Yavneh 1998; Vanneste and Yavneh 2004) on an $f$ plane suggests that rotation does not affect the basic characteristics of the excitation mechanism studied in this work and that despite the simplified model used, nonnormal interaction of vorticity and internal wave manifolds in the presence of shear is expected to play a significant role in the process of spontaneous gravity wave emission from highly sheared regions arising during baroclinic life cycles (Plougonven and Snyder 2007). Investigation of the role of the excitation mechanism and nonorthogonality between vorticity and gravity wave manifolds for more realistic flows will be the subject of future work.

*Acknowledgments.* The authors thank two anonymous reviewers for their useful comments and numerous suggestions, which helped to improve the manuscript. This research was supported by NSF ATM-0736022.

## APPENDIX A

### Particular Solution in the Weak Coupling Regime

To calculate the particular solution (2) in the weak coupling regime [$(m/k) \ll S^{1/2}$], we use the Wentzel–Kramers–Brillouin (WKB) asymptotic approximation to the homogeneous equation that was found in Part I:

$$\phi_{\pm} = S^{-1/4}\sqrt{\omega(t)}e^{\pm i\sqrt{S}\int_0^t \omega(s)ds} + O[(m/k)S^{-1/2}], \quad \text{(A1)}$$

where $Q$ and $\omega$ are given by (22) and (12) in Part I, respectively. The Wronskian of these solutions is

$$W = \phi_+ \frac{d\phi_-}{dt} - \phi_- \frac{d\phi_+}{dt} = -2i\omega^2, \qquad \text{(A2)}$$

yielding the particular solution (2), where $\phi_\pm$ and $W$ are given by (A1) and (A2), respectively. For $S \gg 1$, $\phi_\pm$ is a rapidly oscillating function, and the leading order in $S$ of the integrals in (2) is obtained using integration by parts

$$\int_0^t \frac{\phi_\pm(s)a(s)}{W(s)}ds = -\frac{km^2}{iS^{1/4}}\int_0^t e^{\pm i\sqrt{S}\int_0^s \omega(\tau)d\tau}\frac{\sqrt{\omega(s)}}{[k^2+(l-ks)^2]^2}ds$$
$$= \frac{\pm km^2 e^{\pm i\sqrt{S}\int_0^t \omega(s)ds}}{S^{3/4}[k^2+(l-kt)^2]^2\sqrt{\omega(t)}} \mp \frac{km^2}{S^{3/4}(k^2+l^2)^2\sqrt{\omega(0)}} + O(S^{-5/4}).$$

So, the particular solution is given to leading order by (4).

## APPENDIX B

### Analysis of the Generation of Exponentially Small Gravity Waves as a Stokes Phenomenon

Vanneste and Yavneh (2004) found in their study of linearized, sheared disturbances on an $f$ plane that inertia–gravity waves were spontaneously generated by balanced initial conditions and that this could be analyzed as a Stokes phenomenon (Olver 1974; Berry 1989): the subdominant homogeneous solution was excited by the dominant, oscillation-free, inhomogeneous solution when time $t$ crossed a Stokes line. The Stokes line arose from singularities of the asymptotic expansion of the solution in the complex $t$ plane. To examine this possibility in our case, we analyze the asymptotic expansion (3) near its singularities in the complex $t$ plane at $t_\pm = l/k \pm i$. Note that the homogeneous solution given by (24) in Part I is singular at $t_\pm$ as well. The Stokes lines are defined as the asymptotes of the curves $\mathrm{Im}\int\omega(s)ds = 0$ as $t \to t_\pm$. Close to $t_\pm$,

$$\omega = \frac{\sqrt{k^2+(l-kt)^2}}{\sqrt{k^2+m^2+(l-kt)^2}} \simeq \frac{k\sqrt{2}}{m}e^{\pm i\pi/4}(t-t_\pm)^{1/2},$$

and the Stokes lines are therefore tangent to

$$S_1 : \arg(t-t_\pm) = \mp\frac{5\pi}{6}, \quad S_2 : \arg(t-t_\pm) = \mp\frac{\pi}{6}, \quad S_3 : \arg(t-t_\pm) = \mp\frac{\pi}{2}.$$

We see that for real $t$, $S_3$ is crossed when time takes the value $l/k$, and as a result we expect the spontaneous generation of gravity waves through a Stokes phenomenon.

To calculate the amplitude of the generated waves, we follow the analysis in Vanneste and Yavneh (2004) and integrate (10) in Part I on a path in the complex plane that comes close to $t_\pm$. We first proceed with the integration near $t_+$ and divide the complex $t$ plane into three regions: the outer regions I and II with $|t-t_+| \gg 1$ and $(t-t_+) < 0$, $(t-t_+) > 0$, respectively, and the inner region III with $|t-t_+| \sim O(1)$. Because our focus is on wave generation by oscillation-free initial conditions, we take the solution in region I to be

$$\hat{\rho}_I = \frac{2mk^2\hat{q}(0)}{iS[k^2+(l-kt)^2]^2},$$

whereas the solution in region II contains the generated gravity waves

$$\hat{\rho}_{II} = \frac{2mk^2\hat{q}(0)}{iS[k^2+(l-kt)^2]^2} + A\sqrt{\omega}e^{i\sqrt{S}\int_0^t \omega(s)ds} + B\sqrt{\omega}e^{-i\sqrt{S}\int_0^t \omega(s)ds}, \qquad \text{(B1)}$$

with amplitudes $A$, $B$ to be determined. In the inner region, the WKB approximation to the homogeneous solution (gravity waves) breaks down, and (10) in Part I needs to be rescaled to obtain the proper balance between the terms in the differential equation. Once the solution in region III is determined, the gravity wave amplitudes are calculated by matching the solution in the inner region, where they are generated, to the solution in the outer regions.

We choose the path of integration close to $t_+$ to be given by the Stokes lines $S_1$ and $S_2$ so that the WKB terms in (B1) have a constant amplitude at leading order. When approaching $t_+$ following $S_1$, the outer solution is given by

$$\hat{\rho}_I = -\frac{2imk^2\hat{q}(0)}{S[k^2+(l-kt)^2]^2} \simeq \frac{im\hat{q}(0)}{2k^2S(t-t_+)^2}. \qquad \text{(B2)}$$

To find the outer solution following $S_2$, we first calculate the phase integral of the gravity waves:

$$\int_0^t \omega(s)ds = \int_0^{l/k} \omega(s)ds + \int_{l/k}^{t_+} \omega(s)ds + \int_{t_+}^t \omega(s)ds \simeq \phi_0 + i\beta + \frac{2}{3} b^{1/2} e^{i\pi/4} (t - t_+)^{3/2}, \tag{B3}$$

where $b = 2k^2/m^2$,

$$\phi_0 = \int_0^{l/k} \omega(s)ds, \tag{B4}$$

is a constant phase shift, and

$$\beta = \frac{1}{i} \int_{l/k}^{t_+} \omega(s)ds = \int_0^1 \left[ \frac{1 - s^2}{1 + (m/k)^2 - s^2} \right]^{1/2} ds. \tag{B5}$$

The value of $\beta$ can be calculated using elliptical functions. Its upper bound is one, and it can be readily shown that its asymptotic values for $m/k \gg 1$ and $m/k \ll 1$ are $\beta \simeq k\pi/(4m)$ and $\beta \simeq 1$, respectively. Introducing (B3) into (B1), we find that on $S_2$,

$$\hat{\rho}_{II} \simeq b^{1/4} e^{i\pi/8} (t - t_+)^{1/4} \{ A e^{\sqrt{S}[i\phi_0 - \beta + (2/3) b^{1/2} e^{3i\pi/4} (t - t_+)^{3/2}]} + B e^{\sqrt{S}[-i\phi_0 + \beta + (2/3) b^{1/2} e^{-i\pi/4} (t - t_+)^{3/2}]} \} + \frac{im\hat{q}(0)}{2k^2 S (t - t_+)^2}. \tag{B6}$$

In region III, the WKB approximation is not valid because there is a turning point at $t = t_+$. The proper balancing of terms in the differential equation determining the evolution of $\hat{\rho}$ in this inner region is obtained by rescaling time according to

$$t = t_+ + (bS)^{-1/3} \tau, \tag{B7}$$

and $\hat{\rho}$ by $\hat{\rho}(\tau) = b^{-2/3} S^{-1/3} \phi(\tau)$, to reduce (10) in Part I at leading order to

$$\frac{d^2\phi}{d\tau^2} - \frac{1}{\tau} \frac{d\phi}{d\tau} + i\tau\phi = -\frac{b^{1/3} \hat{q}(0)}{m\tau}. \tag{B8}$$

The solution of (B8) is given in terms of derivatives of Scorer functions (Abramowitz and Stegun 1965) $\mathrm{Hi}'(r\tau)$ and $\mathrm{Gi}'(r\tau)$, where $r^3 = i$. Matching the solution of (B8) to $\hat{\rho}_I$ on $S_1$, proceeds from using the asymptotic expressions for Hi′ and Gi′ following $S_1$; that is, for $\tau = e^{-5i\pi/6}|\tau|$ when $|\tau| \gg 1$. It can be readily shown that the solution matching (B2) is

$$\phi = \frac{\pi b^{1/3} e^{i\pi/6} \hat{q}(0)}{m} \mathrm{Hi}'(e^{-i\pi/6}\tau). \tag{B9}$$

To find the asymptotic behavior of (B9) on $S_2$ and match with (B6), we use the connection formula

$$\mathrm{Hi}'(e^{-i\pi/6}\tau) = e^{-4i\pi/3} \mathrm{Hi}'(e^{-5i\pi/6}\tau) + 2e^{5i\pi/6} \mathrm{Ai}'(i\tau).$$

Following $S_2$, $\tau = e^{-i\pi/6}|\tau|$ and for $|\tau| \gg 1$, the asymptotic expression of (B9) becomes

$$\phi = \frac{\pi b^{1/3} e^{i\pi/6} \hat{q}(0)}{m} \mathrm{Hi}'(e^{-i\pi/3}|\tau|) \simeq \frac{b^{1/3} e^{-7i\pi/6} \hat{q}(0)}{m|\tau|^2} + \frac{\sqrt{\pi} b^{1/3} e^{i\pi/8} \hat{q}(0)}{m} \tau^{1/4} e^{(2/3) e^{-i\pi/4} \tau^{3/2}},$$

yielding

$$\hat{\rho}_{III} \simeq -\frac{\hat{q}(0) e^{-i\pi/6}}{(2mk^2 S)^{1/3} |\tau|^2} + \frac{\hat{q}(0) \sqrt{\pi} e^{i\pi/8}}{(2mk^2 S)^{1/3}} \tau^{1/4} e^{(2/3) e^{-i\pi/4} \tau^{3/2}}. \tag{B10}$$

Taking (B7) into account, (B6) becomes

$$\hat{\rho}_{II} = -\frac{\hat{q}(0) e^{-i\pi/6}}{(2mk^2 S)^{1/3} |\tau|^2} + \frac{b^{1/6} e^{i\pi/8}}{S^{1/12}} \tau^{1/4} \times [A e^{\sqrt{S}(i\phi_0 - \beta) + (2/3) e^{3i\pi/4} \tau^{3/2}} + B e^{\sqrt{S}(-i\phi_0 + \beta) + (2/3) e^{-i\pi/4} \tau^{3/2}}].$$

Matching with (B10) yields

$$[A, B] = \left[ 0, \frac{\hat{q}(0) \sqrt{\pi} e^{\sqrt{S}(i\phi_0 - \beta)}}{k\sqrt{2} S^{1/4}} \right]. \tag{B11}$$

Following the same procedure, we can find the contribution from $t_-$ and finally obtain the solution given by (5).

## APPENDIX C

### Particular Solution in the Strong Coupling Regime

In appendix B, we found that gravity wave excitation could be analyzed as a Stokes phenomenon and that gravity waves were excited with amplitude $O[\exp(-\beta\sqrt{S})]$. For $m/k$, $S \gg 1$ with $(m/k)\ O(S^{1/2})$, it can be readily shown from (B5) that $\beta\sqrt{S} \simeq \sqrt{S}\pi/4(m/k)$, and these waves are therefore of order one. The purpose of this appendix is to accurately calculate their amplitude. Although a sophisticated technique of exponential asymptotics based on resurgence can be applied to obtain the amplitude of the waves for $(m/k)\ O(S^{1/2})$ (Ólafsdóttir et al. 2005), we follow a computationally more efficient way and try to

come up with a suitable approximation for the integrals in (2). Even though for $(m/k)$ $O(S^{1/2})$, $Q(t)$ [given by (22) in Part I] is not a slowly varying function of time, the WKB solution given by (23) in Part I provides us with a good approximation for the wave amplitude, which we use to calculate the particular solution that is given by

$$\phi_{\text{part}} = -\frac{k^2 m\hat{q}(0)\omega(t)}{Q(t)^{1/4}}\left[e^{i\int_0^t\sqrt{Q(s)}ds}\int_0^t g(s)e^{-i\int_0^s\sqrt{Q(\tau)}d\tau}ds + e^{-i\int_0^t\sqrt{Q(s)}ds}\int_0^t g(s)e^{i\int_0^s\sqrt{Q(\tau)}d\tau}ds\right], \tag{C1}$$

where

$$g(s) = \frac{\omega(s)}{Q(s)^{1/4}[k^2+(l-ks)^2]^2}.$$

The integrands in (C1) consist of the oscillating function $\exp[\pm i\int_0^t\sqrt{Q(s)}ds]$ multiplied by $g$, a highly localized function around its maximum at $t = l/k$ with a half-width depending on $(m/k)S^{-1/2}$ and varying between 0.6 and 1.4. The value of the integral will therefore depend on the phase oscillation within the envelope of $g$. We first approximate $g$ by the following Gaussian function:

$$\tilde{g}(s) = \frac{e^{-(l-ks)^2\log(2)/(k\delta t)^2}}{k^3[(k^2S+3m^2)(k^2+m^2)]^{1/4}},$$

where $\delta t = \sqrt{\sqrt{2}-1}+e^{-0.35}[1-e^{-0.7(m/k\sqrt{S})}]$ is the Gaussian half-width that was empirically calculated. For $m/k$, $S \gg 1$ with $(m/k)$ $O(S^{1/2})$, $Q$ has a local maximum $Q_{\max} = 3 + 1/\tilde{m}^2$ at $t = l/k$, where $\tilde{m} = m/(k\sqrt{S})$ and two local minima $Q_{\min} \simeq (3/2)6^{1/3}\tilde{m}^{-4/3}$ at approximately $t = l/k \pm \sqrt{6^{1/3}\tilde{m}^{2/3}-1}$. To estimate the values of the integrals in (C1), we approximate $Q$ by its mean within $g$: $Q(t) \simeq Q_m = (1/2)(Q_{\max}+Q_{\min})$. The integrals can be then approximated by

$$\int_0^t g(s)e^{-i\int_0^s\sqrt{Q(t)}dt}ds \simeq \int_0^t \tilde{g}(s)e^{\pm i\sqrt{Q_m}s}ds.$$

Because $g$ is localized around its maximum at $t = l/k$, we can approximate this integral for large times by

$$\int_0^t \tilde{g}(s)e^{\pm i\sqrt{Q_m}s}ds \simeq \int_{-\infty}^{\infty}\tilde{g}(s)e^{\pm i\sqrt{Q_m}s}ds = \frac{\sqrt{\pi}\delta t}{\sqrt{\log(2)}}\frac{e^{\pm iQ_m l/k}e^{-Q_m(\delta t)^2/4\log(2)}}{k^3 m(3+1/\tilde{m}^2)^{1/4}},$$

yielding the particular solution

$$\phi_{\text{part}} = A_{as}\frac{\omega(t)}{Q(t)^{1/4}}[-e^{-iQ_m l/k+i\int_0^t\sqrt{Q(s)}ds} + e^{iQ_m l/k-i\int_0^t\sqrt{Q(s)}ds}], \tag{C2}$$

where

$$A_{as} = \frac{\hat{q}(0)\sqrt{\pi}\delta t}{k\sqrt{\log(2)}(3+1/\tilde{m}^2)^{1/4}}e^{-Q_m(\delta t)^2/4\log(2)}$$

is the amplitude of the forced waves. The relative error of (C2) when compared to the numerical- integrated solution is around 10% for $(m/k)$ $O(S^{1/2})$, whereas it overestimates the forced waves' amplitude by a factor of 2 for $(m/k) \gg S^{1/2}$. Finally, note that for large times these forced waves correspond to vertical vorticity $\zeta_z$ waves with amplitude of $O(mA_{as}/S^{1/2})$, that is, of order $\hat{q}(0)FS^{1/4}$.

## REFERENCES


Abramowwitz, M., and I. A. Stegun, 1965: *Handbook of Mathematical Functions.* Dover, 1064 pp.

Bakas, N. A., and B. F. Farrell, 2009: Gravity waves in a barotropic shear flow. Part I: Growth mechanisms in the absence of potential vorticity perturbations. *J. Phys. Oceanogr.,* **39,** 481–496.

——, P. J. Ioannou, and G. E. Kefaliakos, 2001: The emergence of coherent structures in stratified shear flow. *J. Atmos. Sci.,* **58,** 2790–2806.

Berry, M. V., 1989: Uniform asymptotic smoothing of Stokes's discontinuities. *Proc. Roy. Soc. London,* **A422,** 7–21.

Farrell, B. F., and P. J. Ioannou, 1996: Generalized stability theory. Part I: Autonomous operators. *J. Atmos. Sci.,* **53,** 2025–2040.

Ford, R., 1994: The instability of an axisymmetric vortex with monotonic potential vorticity in rotating shallow water. *J. Fluid Mech.,* **280,** 303–334.

——, M. E. McIntyre, and W. A. Norton, 2000: Balance and the slow quasimanifold: Some explicit results. *J. Atmos. Sci.,* **57,** 1236–1254.

Guest, F. M., M. J. Reeder, C. J. Marks, and D. J. Karoly, 2000: Inertia-gravity waves observed in the lower stratosphere over Macquarie Island. *J. Atmos. Sci.,* **57,** 737–752.

Hakim, V., 1998: Asymptotic techniques in nonlinear problems: Some illustrative examples. *Hydrodynamics and Nonlinear Instabilities,* C. Godreche and P. Manneville, Eds., Cambridge University Press, 295–386.

Kalashnik, M. V., G. R. Mamatsashvili, G. D. Chagelishvili, and J. G. Lominadze, 2006: Linear dynamics of non-symmetric perturbations in geostrophic horizontal shear flows. *Quart. J. Roy. Meteor. Soc.,* **132,** 505–518.

Kuhlbrodt, T., A. Griesel, M. Montoya, A. Levermann, M. Hofmann, and S. Rahmstorf, 2007: On the driving processes of the Atlantic meridional overturning circulation. *Rev. Geophys.,* **45,** RG2001, doi:10.1029/2004RG000166.

Lighthill, M. J., 1952: On sound generated aerodynamically, I. General theory. *Proc. Roy. Soc. London,* **A421,** 564–587.

McWilliams, J. C., and I. Yavneh, 1998: Fluctuation growth and instability associated with a singularity of the balance equations. *Phys. Fluids,* **10,** 2587–2596.

Ólafsdóttir, E. I., A. B. Olde Daalhuis, and J. Vanneste, 2005: Stokes-multiplier expansion in an inhomogeneous differential equation with a small parameter. *Proc. Roy. Soc. London,* **A461,** 2243–2256.

Olver, F. W. J., 1974: *Asymptotics and Special Functions*. Academic Press, 572 pp.

Orr, W. M. F., 1907: The stability or instability of the steady motions of a perfect liquid and of a viscous liquid. *Proc. Roy. Irish Acad. Ser. A,* **27,** 9.

O'Sullivan, D., and T. J. Dunkerton, 1995: Generation of inertia-gravity waves in a simulated life cycle of baroclinic instability. *J. Atmos. Sci.,* **52,** 3695–3716.

Pavelin, E., J. Whiteway, and G. Vaughan, 2001: Observation of gravity wave generation and breaking in the lowermost stratosphere. *J. Geophys. Res.,* **106,** 5173–5179.

Plougonven, R., and V. Zeitlin, 2002: Internal gravity wave emission from a pancake vortex: An example of wave–vortex interaction in strongly stratified flows. *Phys. Fluids,* **14,** 1259–1268.

——, and C. Snyder, 2007: Inertia-gravity waves spontaneously generated by jets and fronts. Part I: Different baroclinic life cycles. *J. Atmos. Sci.,* **64,** 2502–2520.

——, H. Teitelbaum, and V. Zeitlin, 2003: Inertia gravity wave generation by the tropospheric midlatitude jet as given by the Fronts and Atlantic Storm-Track Experiment radio soundings. *J. Geophys. Res.,* **108,** 4686, doi:10.1029/2003JD003535.

Uccellini, L. W., and S. E. Koch, 1987: The synoptic setting and possible energy sources for mesoscale wave disturbances. *Mon. Wea. Rev.,* **115,** 721–729.

Vanneste, J., 2004: Inertia–gravity wave generation by balanced motion: Revisiting the Lorenz–Krishnamurthy model. *J. Atmos. Sci.,* **61,** 224–234.

——, and I. Yavneh, 2004: Exponentially small inertia-gravity waves and the breakdown of quasigeostrophic balance. *J. Atmos. Sci.,* **61,** 211–223.

Viudez, A., and D. G. Dritschel, 2006: Spontaneous emission of inertia–gravity wave packets by balanced geophysical wave packets. *J. Fluid Mech.,* **553,** 107–117.

Zhang, F., 2004: Generation of mesoscale gravity waves in upper-tropospheric jet-front systems. *J. Atmos. Sci.,* **61,** 440–457.